

连续变焦微型液体柱透镜系统的设计与制备

盛树武¹, 呼德港¹, 周琰武¹, 王丹阳¹, 孙丽存^{1,2*}¹云南师范大学物理与电子信息学院, 云南 昆明 650500;²云南省光电信息与技术重点实验室, 云南 昆明 650500

摘要 设计并制备了一种具有较大变倍比及较高成像质量的充液式连续变焦微型柱透镜系统。该系统由埋入聚二甲基硅氧烷基片的两片对称弯月柱透镜及一片双凸柱透镜构成; 两弯月柱透镜边缘位置胶合形成空腔, 改变注入其中的液体折射率, 可实现柱透镜系统的连续变焦; 双凸柱透镜的优化设计可控制柱透镜系统整个变焦范围内的像差。当柱透镜系统中注入的液体折射率由 1.3330 变化到 1.5530 时, 可实现系统后焦距由 52.292~4.972 mm 的连续平滑变化。整个变焦范围内, 柱透镜系统径向弥散斑均方根半径始终小于 5 μm , 接近衍射极限。对柱透镜系统的可能公差进行了详细分析, 证实了该设计的可行性, 并完成了透镜系统的加工制备及后焦距、调制传递函数曲线的测量。该变焦系统具有变倍比高、体积小、结构简单稳定、成像质量高等优势, 可用于集成化的微型设备中。

关键词 光学设计与制备; 变焦系统; 液体柱透镜; 成像质量

中图分类号 O435 **文献标志码** A

DOI: 10.3788/AOS230540

1 引言

变焦透镜是一种极其重要的光学元件, 其在光通信^[1-2]、光学成像^[3-4]和生物医学检测^[5-7]等领域的应用逐渐不可替代。液态变焦透镜用液体作为光学介质, 在外界因素(例如压力、电场等)^[8-10]发生改变时, 液体的折射率或形状将发生改变, 实现焦距的自动调节, 相较于传统的机械变焦透镜具有结构紧凑易集成、无机械磨损、控制灵活等优点^[11-14], 已然成为当前的研究热点。目前, 常见的液态透镜主要有 3 种: 基于电润湿效应的液态变焦透镜^[15-17]、液晶变焦透镜^[18-20]和充液型变焦透镜^[21-22]。前两种方法都需要电压控制, 且电润湿效应需要较高的驱动电压, 工艺复杂, 镜头光轴的稳定性很难保证, 而液晶的通光率较差、光学失真较大。相较而言, 充液型变焦透镜具有调节方式多样、焦距变化范围大等优点。然而, 目前关于变焦透镜的研究大部分集中于常用的球对称变焦透镜, 对于在光束操控方面具有不可或缺作用的柱透镜^[23-24]却研究较少。

为此, 本课题组设计了一系列的液芯变焦柱透镜^[25-26], 通过改变充入透镜空心区域的液体种类或浓度改变液体的折射率, 进而实现透镜焦距的改变, 属于充液型变焦透镜。文献[25]中所设计的复合型液芯柱透镜尺寸较大, 不易于集成, 文献[26]中的微型柱透镜

系统焦距过短、变焦范围较小, 应用范围受限。因此, 本文以文献[26]的透镜结构为初始结构, 对其进行 4 倍放缩, 设计并制备了一种基于聚二甲基硅氧烷(PDMS)基片的新型液体变焦柱透镜系统, 该系统兼具变倍比高、结构稳定、易于集成等优势。所提连续变焦微型液体柱透镜系统可用来替代光束整形、扫描成像等系统中的定焦柱透镜, 为光束操控提供更高的自由度及适应性, 也可将其应用于液体折射率及液相扩散系数的准确测量^[27]。

2 透镜设计与优化

液体变焦柱透镜系统的设计流程如图 1 所示, 主要包括初始结构的建立及优化、成像质量评估、公差分析及加工制备几个环节。

光学设计中可通过分配初级像差的方法计算透镜系统的初始结构, 也可选用现有专利或文章中的透镜结构作为初始结构。本研究选用文献[26]中详细介绍的基于 PDMS 基片的微流控液芯柱透镜作为原始结构并进行优化。该原始结构由埋入方形 PDMS 基片(5.0 mm×2.0 mm×4.6 mm)的毛细管及双凸柱透镜组成: 毛细管管壁为 H-K9L 玻璃, 外半径为 1.00 mm, 内半径为 0.70 mm, 毛细管前壁与 PDMS 基片前壁的间距为 0.30 mm; 双凸柱透镜为 F2 玻璃, 前后表面的

收稿日期: 2023-02-13; 修回日期: 2023-03-20; 录用日期: 2023-04-06; 网络首发日期: 2023-04-16

基金项目: 国家自然科学基金(62065019, 61705192)、云南省高层次科技人才及创新团队选拔专项-中青年学术和技术带头人后备人才项目(202205AC160029)

通信作者: *aliceckczy@163.com

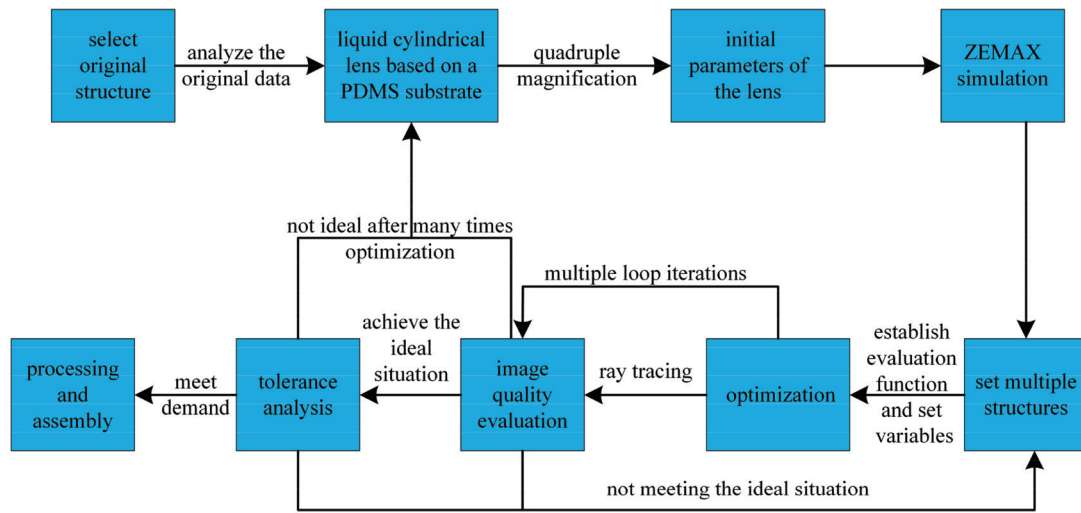


图 1 设计流程图

Fig. 1 Flow chart of design procedure

曲率半径分别为 1.40 mm、-1.10 mm，厚度为 1.10 mm，其前表面与毛细管后壁密接，后表面与 PDMS 基片后壁的间距为 1.60 mm。该原始结构可以通过改变毛细管中注入液体的折射率实现变焦，但是由于尺寸限制，其焦距变化范围较小且始终小于 10 mm，难以实际应用。

因此，对该原始结构进行 4 倍放大后作为初始结构，将对应参数输入 ZEMAX 光学仿真软件进行优化。本变焦系统中充入不同折射率的液体时其焦距不同，可将其视为变焦系统的不同结构。在 ZEMAX 中构建多重结构，将变焦系统中柱透镜的曲率半径、厚度及玻璃材料种类均设为变量，并设定评价函数，对其进行迭代优化，直到获得在整个变焦范围内成像质量均良好的透镜系统。变焦系统最终结构如图 2 所示，由埋入 PDMS 基片 (14.7 mm × 6.0 mm × 10.0 mm) 的两片对称弯月柱透镜 (H-LAK3 玻璃) 及一片双凸柱透镜 (H-LAF50B 玻璃) 组成，两片对称弯月柱透镜边缘胶合后形成可注入液体的空腔，具体参数如表 1 所示。

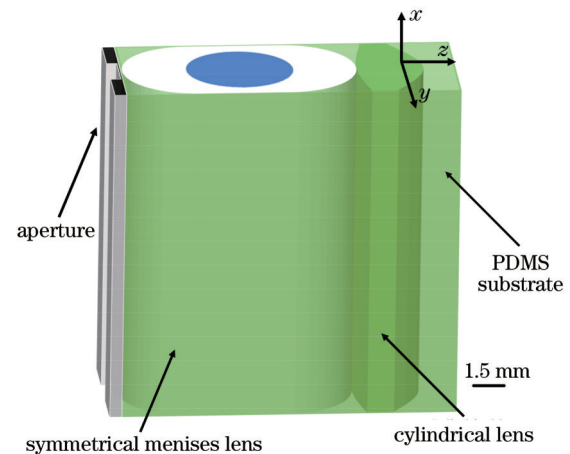


图 2 基于 PDMS 基片的液体变焦柱透镜最终结构

Fig. 2 Final structure of the liquid zoom cylindrical lens based on a PDMS substrate

3 变焦能力和成像质量分析

成像系统后焦距 f_b 易于测量，便于指导光学系统的搭建，而有效焦距 f 可用来反映系统的成像性能。本研究对这两个参数进行了分析，用以展示所设计的

表 1 基于 PDMS 基片的液体变焦柱透镜最终结构参数

Table 1 The final structure parameters of the liquid zoom cylindrical lens based on a PDMS substrate

No.	Surface type	Radius /mm	Thickness /mm	Glass	Refractive index ($\lambda=589$ nm)	Semidiameter /mm
1	Toroidal	Infinity	0	PDMS	1.4115	3.0
2	Toroidal	3.0	3.1	H-LAK3	1.7469	3.0
3	Toroidal	2.0	4.0	Liquid	1.3330-1.5530	2.0
4	Toroidal	-2.0	3.1	H-LAK3	1.7469	2.0
5	Toroidal	-3.0	0	PDMS	1.4115	3.0
6	Toroidal	15.7	3.0	H-LAF50B	1.7725	3.0
7	Toroidal	-6.0	1.5	PDMS	1.4115	3.0
8	Toroidal	Infinity		Atmosphere	1.0000	3.0

微型液体柱透镜系统的变焦能力。由于柱透镜只在其径向方向对光线具有屈光作用,因此涉及的焦距均为其径向(即图 2 中 Y 方向)焦距。所设计的柱透镜系统共包括 8 个折射曲面,即 PDMS 基片的前后表面、对称弯月柱透镜的 4 个曲面以及双凸柱透镜的 2 个曲面,利用逐面成像法,根据高斯光学可知其后焦距 f_B 的表达式为

$$f_B = s'_8, \quad (1)$$

$$\frac{n'_i}{s'_i} - \frac{n_i}{s_i} = \frac{n'_i - n_i}{R_i}, \quad i = 1, 2, \dots, 8, \quad (2)$$

$$s_{i+1} = s'_i - d_i, \quad i = 1, 2, \dots, 7, \quad (3)$$

$$s_1 = \infty, \quad (4)$$

式中: R_i 为第 i 个曲面的曲率半径; s_i, s'_i 分别为柱透镜系统第 i 个曲面的物距与像距, s'_8 即为微流控芯片柱透镜的后焦距, 记为 f_B ; n_i 和 n'_i 分别为第 i 个折射面物方空间和像方空间的折射率; d_i 是相邻光学表面之间的轴向距离。同时, 近轴光学系统的有效焦距 f 可表示为

$$f = \frac{D/2}{u'_8}, \quad (5)$$

$$u'_i = \frac{s_i u_i}{s'_i}, \quad i = 3, 4, \dots, 8, \quad (6)$$

$$u_{i+1} = u'_i, \quad i = 2, 3, \dots, 7, \quad (7)$$

$$u'_2 = u_2 + i_2 - i'_2, \quad (8)$$

$$i'_2 = \frac{n_2 i_2}{n'_2}, \quad (9)$$

$$i_2 = \frac{D/2}{R_2}, \quad (10)$$

$$u_2 = 0, \quad (11)$$

式中: D 代表通光孔径直径大小; u_i, u'_i 分别代表第 i 个光学曲面的物方孔径角及像方孔径角; i_2, i'_2 分别代表第 2 个面的入射角及折射角。

由式(2)可知, 柱透镜系统第 3 个表面的像距随注入对称弯月柱透镜芯区液体折射率的变化而变化, 进而影响后续表面的物距和像距, 因此后焦距 f_B 和有效焦距 f 均为液体折射率 n 的函数。将表 1 所列透镜参数及原始结构参数代入上述递推公式, 可得两变焦系统 f_B 和 f 的变化曲线, 具体如图 3 所示。可以明显看出, 所设计的新型充液柱透镜系统有着更优越的变倍比, 当柱透镜系统中注入的液体折射率由 1.3330 变化到 1.5530 时, 其焦距 f 由 35.090 mm 连续平滑地减小到 9.164 mm, 后焦距 f_B 相应地从 52.292 mm 下降到 4.972 mm。

所设计的液体柱透镜系统在 4 种不同焦距结构下的仿真图如图 4 所示。图 4(a)~(d) 给出了当入射光沿 Y 方向宽度为 2.4 mm 时, 分别填充不同折射率液体的柱透镜系统在 y - z 平面上的光线追迹图, 直观地展示了其变焦能力。图 4(e)~(h) 为相应的像差扇形图, 表明在整个焦距范围内, 系统最大孔径边缘像差控制在 20 μm 以内。

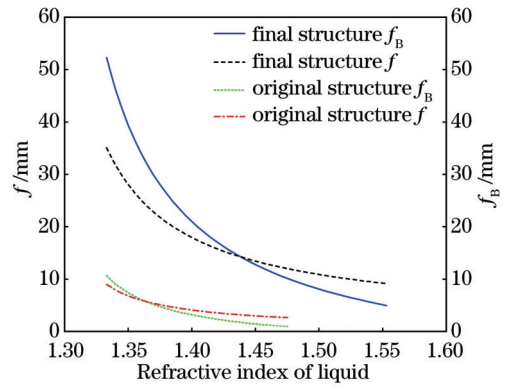


图 3 两种液体柱透镜系统后焦距和焦距随注入溶液折射率变化的曲线

Fig. 3 The curves of the back focal length and focal length of the two kinds of liquid cylindrical lenses system as a function of the liquid refractive index

入射孔径宽度为 2.4 mm 时, 变焦柱透镜焦平面 Y 方向的均方根(RMS)半径和峰-谷波前像差如图 5 所示。Y 方向均方根半径始终小于 5 μm , 小于艾里光斑半径, 与常用的图像接收器件的像元大小数量级相同。当后焦距在 6.195~11.720 mm 和 36.627~52.292 mm 之间时, Y 方向的峰-谷波前像差小于 $\lambda/4$ (图 5 中水平虚线所示), 成像质量接近衍射极限。

不同变焦状态下液体柱透镜的调制传递函数(MTF)曲线如图 6 所示。由图 6(a)、(c) 可以看出, 当液体折射率为 1.3330 和 1.4730 时, 透镜的 MTF 曲线接近衍射极限, 成像质量优越; 图 6(b)、(d) 表明, 当液体折射率分别为 1.3610 和 1.5530 时, 镜头的 MTF 曲线略有下降, 但依旧有较好的成像质量。图 3~6 表明, 所设计的微型液芯柱透镜在整个变焦范围内保持较高成像质量。

4 公差分析

着重考虑镜片加工成形过程中各表面曲率半径和厚度的偏差以及安装过程对称弯月透镜(SL)和双凸柱透镜(CL)的倾斜和偏心对成像质量的影响。选择反映柱透镜系统焦斑大小的 Y 方向均方根光斑半径作为评价标准, 对各误差参数的敏感性进行分析, 对综合公差进行蒙特卡罗分析, 用以指导加工制备。

依据目前国内柱透镜加工工艺水平, 设置弯月柱透镜及双凸柱透镜每个表面(透镜系统的第 2 表面到第 7 个表面)的曲率半径误差为 $\pm 1\%$, 对应系统焦平面均方根半径随后焦距变化曲线如图 7 所示。可以看出, 第 2 片弯月柱透镜后表面的曲率半径加工公差影响最大, 但整体仍控制在 10 μm 以下。

用同样的分析思路研究了厚度、偏心和倾斜误差的影响, 结果如图 8~10 所示。由图 8 可知, 表面 2、3 和 5~7 的厚度在一般加工精度 (± 0.1 mm) 下可以满足 Y 方向均方根光斑半径的要求, 而表面 4 的厚度误

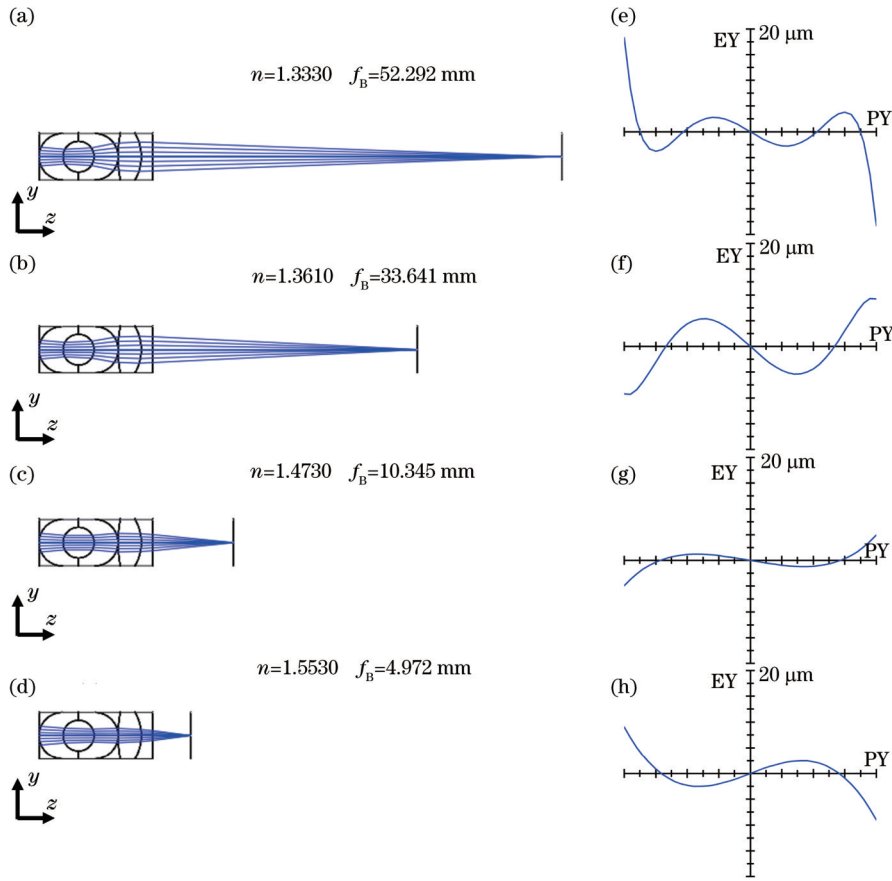


图 4 变焦液体柱透镜的 ZEMAX 仿真结果。(a)~(d)柱透镜 y - z 平面的光线追迹图;(e)~(h)对应的 Y 方向像差扇形图
 Fig. 4 ZEMAX simulation results of the liquid zoom cylindrical lens. (a)-(d) Ray tracing diagrams of the cylindrical lens in y - z plane; (e)-(h) the corresponding spherical aberration curves along the Y direction

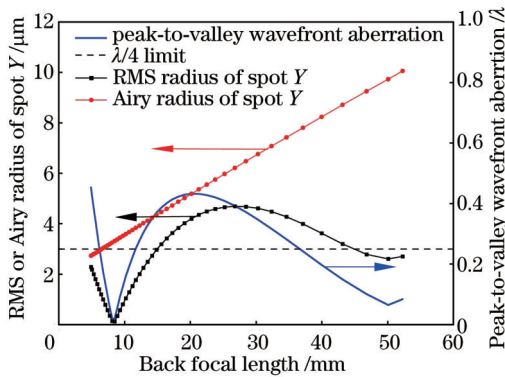


图 5 Y 方向 RMS 半径、艾里光斑半径和峰-谷波前像差图
 Fig. 5 RMS radius, Airy spot radius and peak-to-valley wavefront aberration in the Y direction

差应小于 ± 0.05 mm。由图 9 可知,表面 2~4 和表面 6、7 的偏心误差为 0.03 mm,是可以接受的,而表面 5 的偏心误差应小于 0.01 mm。由图 10 可知,当倾斜误差小于 0.20° 时,安装 SL 和 CL 透镜引起的倾斜误差对 Y 方向均方根半径的影响是可以接受的。

根据灵敏度分析:设置液体柱透镜表面 2~7 曲率半径加工误差为 $\pm 1\%$;表面 2~3 和 5~7 的厚度加工误差为 ± 0.1 mm,表面 4 的厚度误差为 ± 0.05 mm;表

面 2~4 和 6、7 的偏心误差为 0.03 mm,表面 5 的偏心误差为 0.01 mm;透镜安装的倾斜误差均为 0.20° 。对 4 种不同后焦距 ($f_B=52.292$ mm、33.641 mm、10.345 mm、4.972 mm) 结构,分别进行 100 次生产概率模拟。其中:透镜系统中注入丙三醇,后焦距为 10.345 mm 时,透镜系统 Y 方向 RMS 半径的最小预期值为 1.1 μm ,最大预期值为 4.3 μm ,80% 的概率小于 2.4 μm ,整体而言预期成像质量最好;注入无水乙醇,后焦距为 33.641 mm 时,RMS 半径的最小预期值为 3.9 μm ,最大预期值为 12.9 μm ,80% 的概率小于 8.7 μm ,整体而言预期成像质量最差,但弥散斑半径仍能控制在常用 CCD 数字相机的两个像元尺寸。

5 实验设计

上述公差分析表明在现有光学元件的加工和系统装调工艺下,所设计的微型液体柱透镜系统是可行的。将所设计的对称弯月透镜和双凸柱透镜送出加工并自行埋入 PDMS 基片,完成微型液体柱透镜的制备,其俯拍图如图 11 中虚框所示。

搭建光路用以观测基于 PDMS 基片的微型变焦系统的变焦本领及不同变焦状态下的成像质量。图 11 为其 MTF 曲线测量装置:配备垂直刃边分化板(如

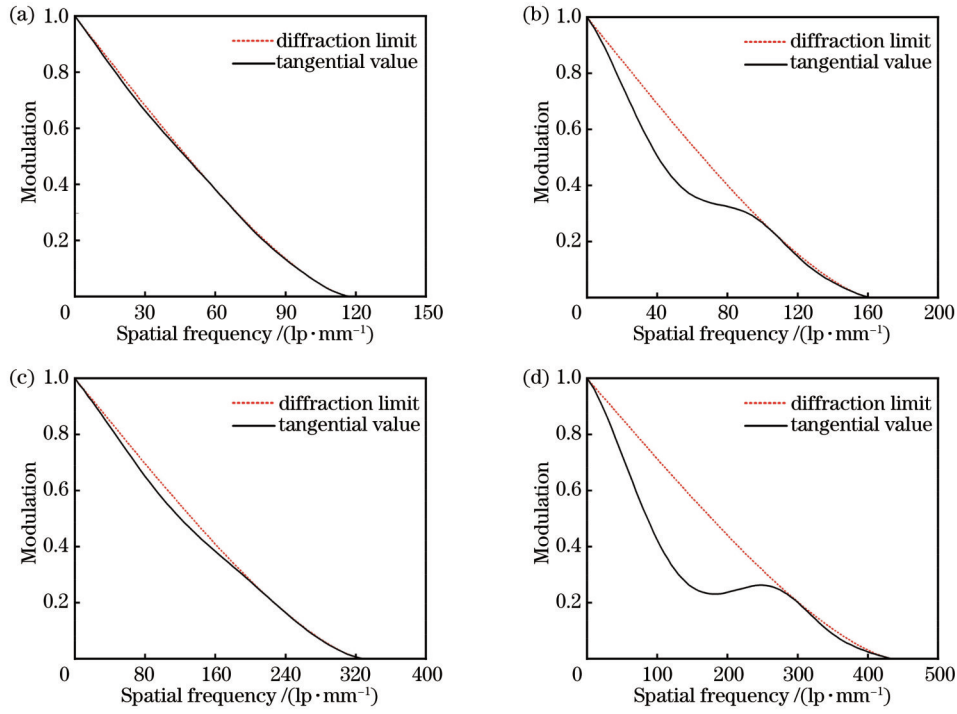


图 6 不同变焦状态下液体柱透镜系统的 MTF 曲线。(a) $n=1.3330, f_b=52.292 \text{ mm}$; (b) $n=1.3610, f_b=33.641 \text{ mm}$; (c) $n=1.4730, f_b=10.345 \text{ mm}$; (d) $n=1.5530, f_b=4.972 \text{ mm}$

Fig. 6 MTF curves of the liquid cylindrical lens under different zoom states. (a) $n=1.3330, f_b=52.292 \text{ mm}$; (b) $n=1.3610, f_b=33.641 \text{ mm}$; (c) $n=1.4730, f_b=10.345 \text{ mm}$; (d) $n=1.5530, f_b=4.972 \text{ mm}$

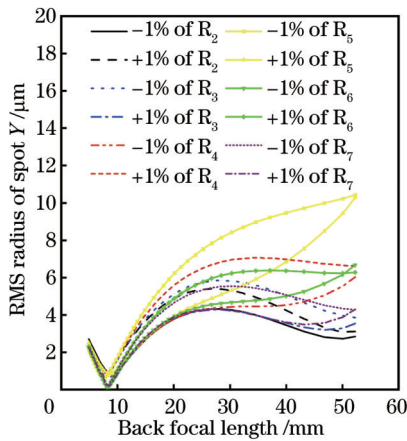


图 7 曲率半径误差为 $\pm 1\%$ 时液体柱透镜 Y 方向 RMS 半径随
后焦距的变化曲线

Fig. 7 Variation in RMS spot radius in the Y direction with back focal length curves for liquid cylindrical lens with $\pm 1\%$ curvature radius errors for each surface

图 11 实框所示)的平行光管发出的单色平行光经光阑限光后垂直照射到基于 PDMS 基片的液体柱透镜系统,经 8 次折射后成像于二维 CCD 阵列。其中:平行光管(中国重庆誉峻科技有限公司生产,型号为 F-550 型平行光管)平行性误差小于等于 $10''$,有效孔径为 50 mm; CCD(大恒图像生产,型号为 MER-2000-19U3M-L)的分辨率为 5496×3672 ,相应的像元尺寸为 $2.4 \mu\text{m} \times 2.4 \mu\text{m}$,接收到的图像经过 USB 接口传

输到计算机,便于观察。变焦透镜后焦距测量装置只需将图 11 中的平行光管替换为文献[27]中所述的激光扩束光源即可,这里不再赘述。

配制折射率($n=1.3330, 1.3450, 1.3600, 1.3800, 1.4100, 1.4350, 1.4750, 1.5150$)不同的 8 种溶液,分别注入对称弯月透镜芯区,采用文献[28]中介绍的标定法测量液体柱透镜系统的后焦距。实验测量值与仿真所得后焦距对比曲线如图 12 所示,测量点与仿真曲线贴合较好,证明了其变焦能力能够达到仿真预期范围。

在对称弯月透镜芯区中依次分别注入折射率为 1.3330(去离子水)、1.3610(无水乙醇)、1.4730(丙三醇)的 3 种液体,沿光轴移动 CCD,直到接收到最为清晰的图像,采用刃边法^[29]测量液体柱透镜的 MTF 曲线。不同充液状态下液体柱透镜系统实验与仿真所得 MTF 对比曲线如图 13 所示,实验 MTF 曲线走向与仿真曲线一致且大部分状态下下降不明显。但是当液体折射率为 1.3610、系统后焦距为 33.641 mm 时,变焦系统的 MTF 曲线下下降较大,尤其在空间频率为 18 lp/mm 时,其下降幅度接近 0.3,与蒙特卡罗分析的预期成像质量相符。以上分析表明,加工完成的连续变焦液体柱透镜系统的成像质量基本能够达到预期设计效果,可将其应用于液体折射率、溶液浓度和液相扩散系数的精确测量。

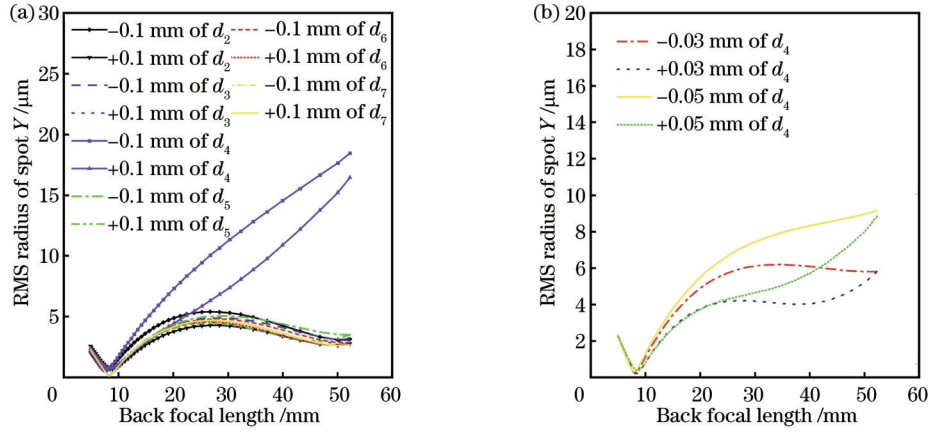


图 8 具有厚度误差的液体柱透镜 Y 方向 RMS 半径随后焦距的变化曲线。(a) 每个曲面误差均为 ± 0.1 mm; (b) 第 4 个曲面具有不同厚度误差

Fig. 8 Variation in RMS spot radius in the Y direction with back focal length curves for liquid cylindrical lens with thickness errors. (a) Error of 0.1 mm for each surface; (b) different thickness errors for the 4th surface

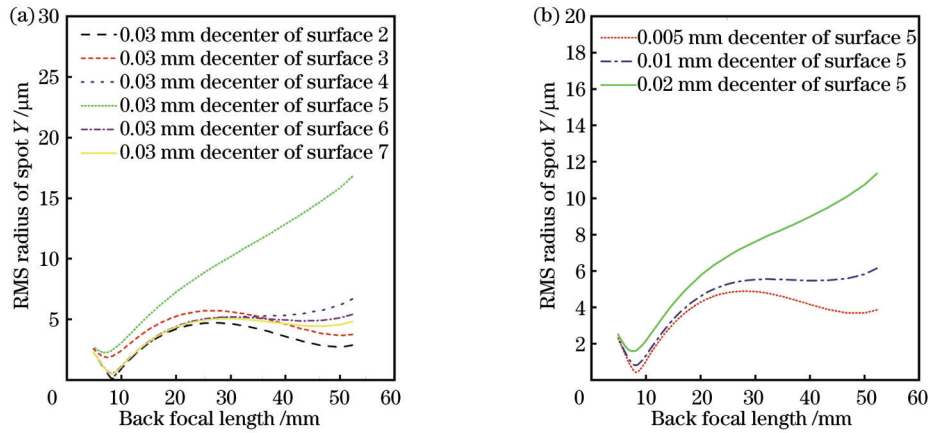


图 9 具有偏心误差的液体柱透镜 Y 方向 RMS 半径随后焦距变化的曲线。(a) 每个曲面误差均为 0.03 mm; (b) 第 5 个曲面具有不同偏心误差

Fig. 9 Variation in RMS spot radius in the Y direction with back focal length curves for liquid cylindrical lens with decentering errors. (a) Error of 0.03 mm for each surface; (b) different decentering errors for the 5th surface

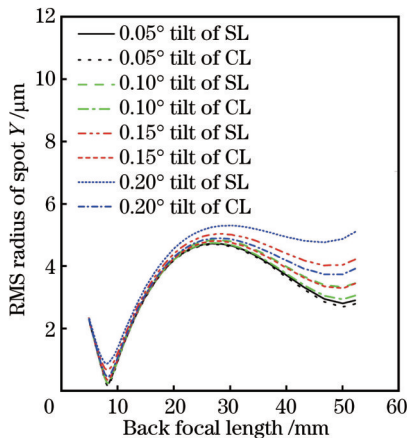


图 10 具有倾斜误差的液体柱透镜 Y 方向 RMS 半径随后焦距的变化曲线

Fig. 10 Variation in RMS spot radius in the Y direction with back focal length curves for liquid cylindrical lens with different tilt errors

6 结 论

设计并制备了一种基于 PDMS 基片的连续变焦微型液体柱透镜系统, 方形 PDMS 基片保障了透镜系统的稳定性。当注入液体的折射率由 1.3330 变为 1.5530 时, 可实现系统后焦距 f_b 由 52.292 mm 到 4.972 mm 连续平滑变化。在整个变焦范围内, 透镜系统的 Y 方向均方根半径始终小于 $5 \mu\text{m}$, 达到了较好的成像质量。与原始结构相比, 在保障了成像质量的前提下, 将变焦范围放大了 5 倍左右。分析了生产和安装误差对透镜系统光学性能的影响, 确定了液芯柱透镜的曲率半径、厚度、偏心和倾斜误差允许的公差范围。在目前的生产 and 安装工艺下, 该液芯柱透镜变焦镜头可以获得理想的成像质量, 具有稳定性好、变焦能力强的特点。

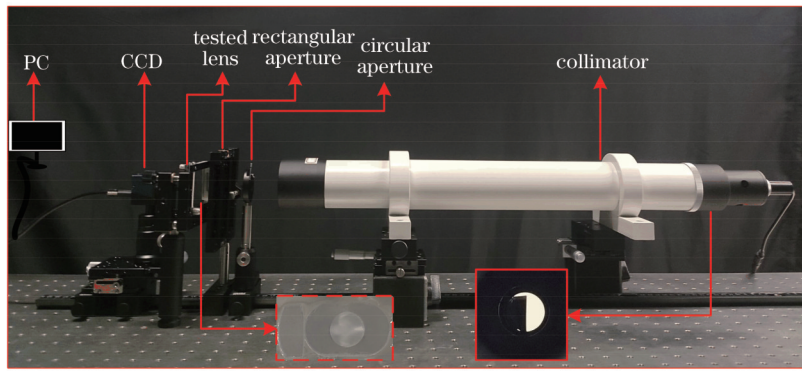


图 11 液体柱透镜系统 MTF 曲线测量装置图

Fig. 11 Experimental device diagram for measuring MTF values of the liquid cylindrical lens system

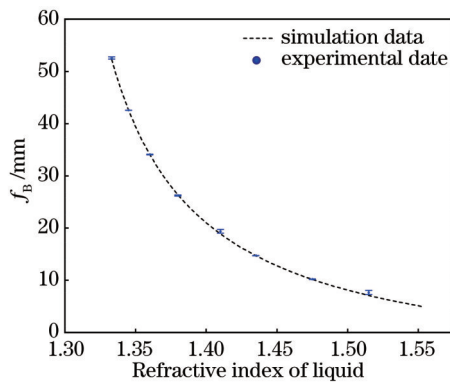


图 12 液体柱透镜系统后焦距随注入溶液折射率的变化曲线
Fig. 12 The curves of the back focal length of the liquid cylindrical lenses system as a function of the liquid refractive index

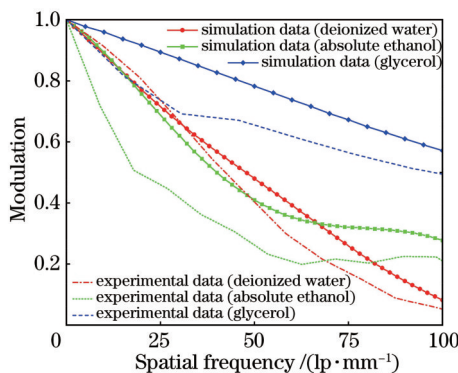


图 13 不同充液状态下柱透镜系统实验与仿真 MTF 曲线对比图
Fig. 13 Comparison of MTF simulation results and experimental results of the cylindrical lens system filled with different refractive index liquids

参 考 文 献

[1] Chronis N, Liu G L, Jeong K H, et al. Tunable liquid-filled microlens array integrated with microfluidic network[J]. Optics Express, 2003, 11(19): 2370-2378.
[2] Wang D, Wang Q H, Shen C, et al. Active optical zoom system [J]. Applied Optics, 2014, 53(31): 7402-7406.
[3] Liang D, Wang X Y. Zoom optical system using tunable

polymer lens[J]. Optics Communications, 2016, 371: 189-195.
[4] Kuiper S, Hendriks B H W. Variable-focus liquid lens for miniature cameras[J]. Applied Physics Letters, 2004, 85(7): 1128-1130.
[5] Dobek K. Motionless microscopy with tunable thermal lens[J]. Optics Express, 2018, 26(4): 3892-3902.
[6] Dong L, Agarwal A K, Beebe D J, et al. Adaptive liquid microlenses activated by stimuli-responsive hydrogels[J]. Nature, 2006, 442(7102): 551-554.
[7] Bae S I, Lee Y, Seo Y H, et al. Antireflective structures on highly flexible and large area elastomer membrane for tunable liquid-filled endoscopic lens[J]. Nanoscale, 2019, 11(3): 856-861.
[8] Binh-Khiem N, Matsumoto K, Shimoyama I. Polymer thin film deposited on liquid for varifocal encapsulated liquid lenses[J]. Applied Physics Letters, 2008, 93(12): 124101.
[9] Park I S, Park Y, Oh S H, et al. Multifunctional liquid lens for variable focus and zoom[J]. Sensors and Actuators A: Physical, 2018, 273: 317-323.
[10] 程阳, 曹杰, 王营博, 等. 介电弹性体驱动液体透镜的设计与分析[J]. 光学学报, 2021, 41(5): 0522004.
Cheng Y, Cao J, Wang Y B, et al. Design and analysis of liquid lens driven by dielectric elastomer[J]. Acta Optica Sinica, 2021, 41(5): 0522004.
[11] 王西玲. 电润湿变焦透镜的焦距及响应时间测量与分析[D]. 南京: 南京邮电大学, 2017.
Wang X L. Measurement and analysis of focal length and response time of electrowetting zoom lens[D]. Nanjing: Nanjing University of Posts and Telecommunications, 2017.
[12] 陈帅. PDMS 薄膜型可变焦液体透镜研究[D]. 杭州: 浙江大学, 2018.
Chen S. Study on PDMS thin film variable focus liquid lens[D]. Hangzhou: Zhejiang University, 2018.
[13] 席崇宾, 黄荣, 周健, 等. 基于液体透镜的激光多普勒信号品质因子增强技术[J]. 中国激光, 2021, 48(7): 0704003.
Xi C B, Huang R, Zhou J, et al. Quality factor enhancement technology of laser Doppler signal based on liquid lens[J]. Chinese Journal of Lasers, 2021, 48(7): 0704003.
[14] 张鹰, 张新, 史广维, 等. 液体透镜在变焦系统中的应用[J]. 中国光学, 2013, 6(1): 46-56.
Zhang Y, Zhang X, Shi G W, et al. Applications of liquid lenses in zoom systems[J]. Chinese Optics, 2013, 6(1): 46-56.
[15] Moghaddam M S, Latifi H, Shahraki H, et al. Simulation, fabrication, and characterization of a tunable electrowetting-based lens with a wedge-shaped PDMS dielectric layer[J]. Applied Optics, 2015, 54(10): 3010-3017.
[16] Berge B, Peseux J. Variable focal lens controlled by an external voltage: an application of electrowetting[J]. The European Physical Journal E, 2000, 3(2): 159-163.
[17] Peng R L, Chen J B, Zhuang S L. Electrowetting-actuated

- zoom lens with spherical-interface liquid lenses[J]. Journal of the Optical Society of America A, 2008, 25(11): 2644-2650.
- [18] 胡轶瑶, 刘志强, 孙涛, 等. 利用液晶透镜实现的局部变焦成像系统[J]. 光学学报, 2022, 42(23): 2311001.
Hu Y Y, Liu Z Q, Sun T, et al. Local zoom imaging system realized by liquid crystal lens[J]. Acta Optica Sinica, 2022, 42(23): 2311001.
- [19] Galstian T, Sova O, Asatryan K, et al. Optical camera with liquid crystal autofocus lens[J]. Optics Express, 2017, 25(24): 29945-29964.
- [20] Ye M, Wang B, Takahashi T, et al. Properties of variable-focus liquid crystal lens and its application in focusing system[J]. Optical Review, 2007, 14(4): 173-175.
- [21] Calixto S, Sánchez-Morales M E, Sánchez-Marin F J, et al. Optofluidic variable focus lenses[J]. Applied Optics, 2009, 48(12): 2308-2314.
- [22] Shaw D, Sun T E. Optical properties of variable-focus liquid-filled optical lenses with different membrane shapes[J]. Optical Engineering, 2007, 46(2): 024002.
- [23] Shi X Y, Meng D J, Qin Z, et al. All-dielectric orthogonal doublet cylindrical metalens in long-wave infrared regions[J]. Optics Express, 2021, 29(3): 3524-3532.
- [24] Ye J S, Gu B Y, Dong B Z, et al. Improved first Rayleigh-Sommerfeld method for analysis of cylindrical microlenses with small f-numbers[J]. Optics Letters, 2004, 29(20): 2345-2347.
- [25] Sun L C, Sheng S W, Meng W D, et al. Design of spherical aberration free liquid-filled cylindrical zoom lenses over a wide focal length range based on ZEMAX[J]. Optics Express, 2020, 28(5): 6806-6819.
- [26] Sun L C, Wang D Y, Guo J, et al. Design and application of a spherical aberration free continuous zoom liquid-filled micro-cylindrical lenses system[J]. Optical Engineering, 2022, 61(8): 085102.
- [27] Sun L C, Meng W D, Pu X Y. New method to measure liquid diffusivity by analyzing an instantaneous diffusion image[J]. Optics Express, 2015, 23(18): 23155-23166.
- [28] Sun L C, Du C, Li Q, et al. Asymmetric liquid-core cylindrical lens used to measure liquid diffusion coefficient[J]. Applied Optics, 2016, 55(8): 2011-2017.
- [29] 孙崇尚, 王琦, 丁亚林, 等. 基于倾斜刃边法航空相机像移的调制传递函数测量[J]. 光学学报, 2014, 34(12): 1212001.
Sun C S, Wang Q, Ding Y L, et al. Modulation transfer function measurement of image motion of aerial camera based on slanted-edge method[J]. Acta Optica Sinica, 2014, 34(12): 1212001.

Design and Fabrication of a Continuous Zoom Liquid Micro-Cylindrical Lens System

Sheng Shuwu¹, Hu Degang¹, Zhou Yanwu¹, Wang Danyang¹, Sun Licun^{1,2*}

¹School of Physics and Electronic Information, Yunnan Normal University, Kunming 650500, Yunnan, China;

²Yunnan Key Laboratory of Opto-Electronic Information Technology, Kunming 650500, Yunnan, China

Abstract

Objective In order to improve the adaptability of cylindrical lenses and expand their application fields, a continuous zoom liquid micro-cylindrical lens system was fabricated. Cylindrical lenses are widely used in engineering fields such as beam shaping, scanning equipment, and holographic display due to their irreplaceable ability in beam manipulation. However, the commonly used focal length of cylindrical lenses is always fixed, and most of the research on zoom systems always focuses on the commonly used symmetric circular lenses, while zoom cylindrical lenses are relatively unexplored. Therefore, a series of liquid zoom cylindrical lenses have been designed in our previous study, including compound-type and capillary-type liquid core zoom cylindrical lenses. They change the refractive index of the core by changing the type or concentration of the liquid filled in the hollow area of the lens and then achieve the variable focal length. However, the compound-type lens has a large size and is not easy to integrate. The capillary-type micro cylindrical lens system has a short focal length and small zoom range, which limit its application. To address the above problems, we aim to design and fabricate a new type of liquid zoom cylindrical lens system based on a polydimethylsiloxane (PDMS) substrate, which is characterized by a high zoom ratio, stable structure, small volume, and easy integration. The continuous zoom liquid micro-cylindrical lens system can be used to replace the fixed focus cylindrical lens in beam manipulation, providing a higher degree of freedom and adaptability and applied in the accurate measurement of liquid refractive index and liquid diffusion coefficient.

Methods The design and fabrication of a continuous zoom liquid micro-cylindrical lens system mainly include four processes: establishment and optimization of the initial structure, zoom ability and imaging quality evaluation, tolerance analysis, and processing and fabrication. In this paper, the capillary-type liquid core micro-cylindrical lens based on a PDMS substrate designed in our previous work is selected as the original structure, and its parameters are quadrupled as the initial structure to lengthen the focal length. When the refractive index of the liquid filled in the capillary varies by changing the type or concentration of the liquid, the focal length of the lens system changes, which can be considered as

the different zoom states of the system and simulated by using the multiple structures in ZEMAX. We set the curvature radii, thicknesses, and glass material types of the cylindrical lens in the zoom system as variables and establish the evaluation function to optimize the system structure iteratively. We also analyze the optimized system's zoom ability and imaging quality until a high zoom ratio and good imaging quality over the zoom range are obtained. Then, the tolerance analysis, including curvature radius, decentering, as well as thickness of every surface in the molding process, and tilting of each cylindrical lens in the installation process, are performed to evaluate the feasibility of the design. We send the designed cylindrical lenses for processing and embed them into a PDMS substrate to complete the preparation. The setup of the observation system is complete, and then the zoom ability and the imaging quality of the continuous zoom liquid micro-cylindrical lens system based on a PDMS substrate are measured to verify the feasibility of the design scheme.

Results and Discussions The zoom lens system we have designed is composed of two symmetrical meniscus lenses and a biconvex cylindrical lens, which are all embedded in a PDMS substrate (Fig. 2). The edges of the two meniscus lenses are glued to form a cavity, and the focal length of the system can be changed continuously by varying the refractive index of the liquid filled in the cavity. The rationally designed biconvex cylindrical lens can control the aberrations of the cylindrical lens system in the whole zoom range. The detailed parameters are listed in Table 1. The dimension of the PDMS substrate is $14.7\text{ mm} \times 6.0\text{ mm} \times 10.0\text{ mm}$. When the refractive index of the liquid injected into the cylindrical lens system changes from 1.3330 to 1.5530, the back focal length of the system changes from 52.292 mm to 4.972 mm continuously and smoothly (Fig. 3). In the whole zoom range, the radial root mean square radius of the diffuse spot of the cylindrical lens system is always less than $5\text{ }\mu\text{m}$ (Fig. 5), and the MTF curves are close to the diffraction limit in most zoom structures (Fig. 6). The possible tolerance of the cylindrical lens system is analyzed in detail (Figs. 7–10), and permissible tolerance is given. Then, the fabrication of the lens system (Fig. 11), as well as the measurement of the back focal length (Fig. 12) and the MTF curves (Fig. 13) are completed. The measured values and curves are close to the simulation results.

Conclusions A continuous zoom liquid micro-cylindrical lens system based on a PDMS substrate is designed and fabricated in this paper, and a cavity is used to inject liquid; a biconvex cylindrical lens is used to control the aberrations, and the square PDMS substrate ensures the stability of the lens system. Both the simulation and measured results have confirmed its high zoom ratio and great imaging quality. Compared with the original structure, the zoom range is enlarged by about 5 times while ensuring the imaging quality. The zoom system has the advantages of a high zoom ratio, small size, simple and stable structure, and high imaging quality, which can be used in integrated micro-devices.

Key words optical design and fabrication; zoom system; liquid cylindrical lens; imaging quality